Received 31 July 2020; revised 7 October 2020; accepted 25 October 2020. Date of publication 2 November 2020; date of current version 28 January 2021.
The review of this article was arranged by Editor C. Surya.

Digital Object Identifier 10.1109/JEDS.2020.3035085

Pixel Parameters Optimization in PWM Image Sensor for Quantization Error Suppression

SILU CHENG [1,2], JIANGTAO XU [1,2] (Member, IEEE), ZHIYUAN GAO [1,2] (Member, IEEE), KAIMING NIE [1,2] (Member, IEEE), XIAOPEI SHI [1,2], AND JIN MIAO [1,2]

1 School of Microelectronics, Tianjin University, Tianjin 30072, China
2 Tianjin Key Laboratory of Imaging and Sensing Microelectronic Technology, Tianjin University, Tianjin 300072, China

CORRESPONDING AUTHOR: J. XU (e-mail: xujiangtao@tju.edu.cn)

This work was supported by the National Key Research and Development Program of China under Grant 2019YFB2204302.

ABSTRACT This article established the error model based on pixel parameters to predict the light intensity quantization error in pulse width modulation (PWM) image sensor, attributed to non-linear response, comparator delay and synchronous reading mechanism. The PWM image sensor encodes light intensity into time interval of consecutive pulses, makes the quantization process of light intensity exceptionally impact the accuracy of the imaging quality. Especially in large pixel array, the synchronous readout scheme introduces quantization error. A PWM image sensor with 400(H) $\times$ 250(V) pixel array was tested to evaluate the model, and the measurements show that the pixel parameters affect the fluctuation of quantization error. With 300lux illuminance and 25μs reading period, the smallest error fluctuation range (11%-15%) can be obtained. The proposed model can suppress the fluctuation of the quantization error in PWM image sensor and help to achieve improved performance of image quality.

INDEX TERMS PWM image sensor, light intensity quantization error, pixel parameters, synchronous reading mechanism.

I. INTRODUCTION

The image sensors quantify the light information as a series of electrical signals. Today, the high-speed dynamic scenes such as automatic driving and target tracking have led to the development of novel topology of image sensor to tackle the problem of redundant information, low accuracy and high power consumption in traditional frame rate image sensor. Inspired by the biological visual system, the “time-based” or “pulse modulation” (PM) image sensor have been realized [1]–[8], which converts the light intensity into the timing of pulses or pulse edges by means of digital pixels, thereby compressing data and increasing working speed. PM imaging essentially divided into two basic techniques, pulse width modulation (PWM) [5]–[8] and pulse frequency modulation (PFM) [1], [2], [4], which derive the time interval between consecutive pulses and the number of pulses in a fixed period, respectively. In comparison with the PWM image sensors, the slow photo-integration speed restrains PFM operation rate. Furthermore, most of the PWM imagers employ the illumination independence in energy consumption, makes the rising demand from the applications in biomedical imaging, industrial machine vision, etc.

Key issue in PM image sensors is the accuracy of light intensity quantization, which mainly affected by the readout circuit and photo-conversion scheme. Pulse pixels based on asynchronous readout inherit the advantages of event-driven and asynchronous processing in biological vision. The pixels only transmit the event pulses of changing information with the asynchronous address event representation (AER) [4], [6], [8]–[13]. Each pixel works independently by outputting changing information orderly with an arbitration mechanism, which ensures the continuous detection of high-speed moving objects with extremely low data volume. The imager in [4] decreases the temporal jitter by reducing fixed pattern noise (FPN), while the jitter due to readout collisions can be decreased by reducing the spike rate per light intensity. The non-ideal factors in high-speed spike-based image sensor are suppressed with the algorithm illustrated in [5], which decreases the standard deviation of the image sensor. The prototype in [6] uses global reset, which is called "time-to–first-spike" encoding scheme [13] to realize lower dynamic power consumption and reduce inefficiency caused by the periodical access requests sent to the bus. The imagers adopt asynchronous readout method, whose light intensity quantization error mainly resulting from the delay of the arbiter are analyzed in detail [8], [10]. A proposed a communication method in [11] could automatically discard aging pulses to reduce the AER arbitration delay error.

However, in higher resolution and higher speed changing scenarios, a large number of trigger events may be generated simultaneously, which will cause the output untimely due to the arbitration mechanism and poor real-time performance. In addition, asynchronous pulse pixels transfer relative scene information (dynamic information) and lack of absolute scene information (static information).

To solve the problem, we focused on the synchronous pulse pixels, while rarely reported. Drawing on the advantages of massive parallelism in biological vision, this kind of pixels carry static and dynamic information row by row under a high frequency scan signal. The design reported in [14] stores the row information in a read-only memory (ROM) and realized the arbitration, supported by that the comparator output is carried to in-pixel DRAM. As the pixel array enlarged, the frequency of the row selection signal will be reduced. Consequently, it makes a great error in quantization of light intensity. The quantization error in PFM image sensor was analyzed in our lab previous work [15]. For a PWM image sensor, the quantization error is effected by various sensor parameters, where the light intensity is inversely proportional to the time interval of consecutive pulses [16], [17]. The results reported in this article are the first study in the quantization error of the light intensity in PWM image sensors. The main effort is on the way to suppression of quantization error to optimize the PWM image sensor design. The synchronous pixels' structure is illustrated in Section II. Section III describes the model of quantization errors affected by the pixel parameters in PWM image sensor. Section IV presents the experimental results and Section V gives the conclusion.

II. PIXEL STRUCTURE

The diagram and integration process of pixel in PWM image sensor are shown in Fig. 1. At the integration stage, the input voltage of the comparator V_d, decreases until lower than the comparator references voltage V_{ref}, and the comparator output V_{com} flips to high. A low-conduction and high-cutoff structure is adopted in the latch, to ensure the output operates synchronized with the clock, thus the output of the NAND gate is the pixel self-reset signal. When the high level of V_{INV} appears, the positive output of RS flip-flop is inverted to high and maintained until the high-frequency reading signal *read* turns on the three-state gate, then V_{RS} is read out of the pixel. The RS flip-flop is reset by *rst* to read the next signal. The value 1 and 0 of OUT indicates

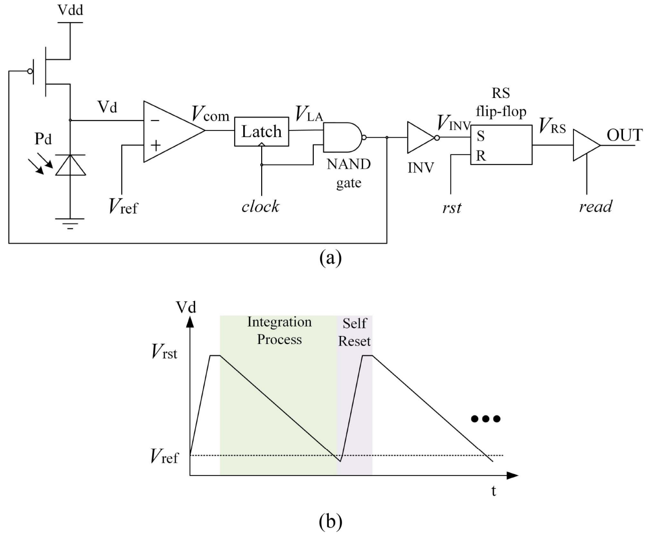

FIGURE 1. Block diagram of pulse pixel and the integration process. (a) Pixel structure of PWM image sensor. (b) Integration process of light intensity.

pulse trigger and no pulse trigger during this reading period, respectively.

In PWM image sensor, the time interval between two adjacent pulses can be used to quantify the light intensity given by

$$I_{ph} = \frac{C_{pd}(V_{rst} - V_{ref})}{\Delta t} \tag{1}$$

where C_{pd} is the photodiode capacitance, V_{rst} is the reset voltage, V_{ref} is the comparator reference voltage, and Δt is the interval time between two adjacent pulses. Equation (1) shows that the light intensity I_{ph} is inversely proportional to the pulse interval Δt.

III. QUANTIZATION ERROR IN PWM IMAGE SENSOR

A. SYNCHRONOUS READING MECHANISM

When the comparator flips over, the pixel does not readout the pulse signal simultaneously, which introduces light intensity quantization error. This error is derived from the time error introduced by the synchronous reset signal and the scanning reading operation.

Synchronous Time Error: The synchronous time error t_{syn} is defined as the interval between the rising edge of V_{com} and the rising edge of the V_{INV}. To analyze the relationship between t_{syn} and the phase of V_{com} and *clock*, we implement four conditions of the synchronous reset signal, and the timing diagram is shown in Fig. 2, T_{LA} is the period of *clock* with duty cycle equals to 1/2.

Scan-Reading Error: Fig. 3 is the timing diagram of the pixels in one row. The period of the signal *read*, T_{read} equals to the period of the signal *rst* T_{rst}. For a PWM image sensor whose pixel array is M(H) × N(V), the duty cycle is set to 1/N, and $T_{read} = T_{rst} = NT_{LA}/2$. Since the reading interval between consecutive pulses is always an integer multiple

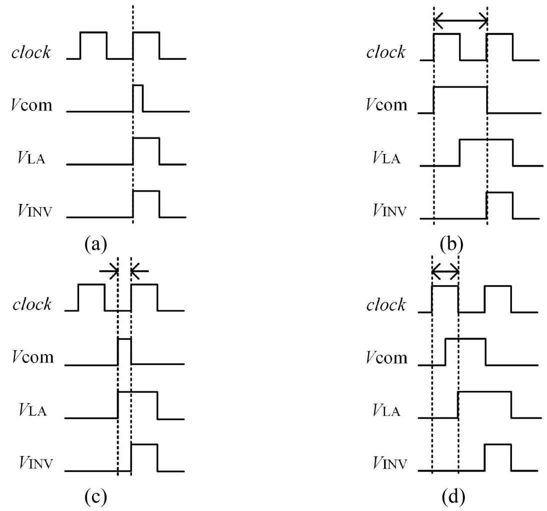

FIGURE 2. **Four conditions of synchronous time error. (a) V_{com} rising edge is coincident with *clock* rising edge, and V_{com} is captured by latch immediately. $t_{syn} = 0$. (b) V_{com} rising edge is coincident with *clock* rising edge, and V_{com} is not captured by latch immediately. $t_{syn} = T_{LA}$. (c) V_{com} rising edge shows up when *clock* remains low. $t_{syn} = 0 \sim T_{LA}/2$. (d) V_{com} shows up when *clock* remains high. $t_{syn} = T_{LA}/2 \sim T_{LA}$.**

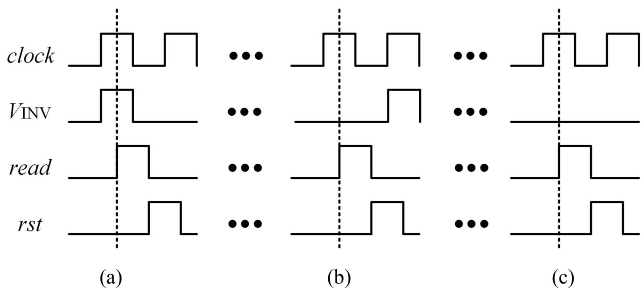

FIGURE 3. **Timing diagram of pixels in one row. From left to right, the scan-reading error $t_{sr} = T_{LA}/4$, $(2N-3)T_{LA}/4$, $5T_{LA}/4$ to $(2N-7)T_{LA}/4$, respectively.**

of T_{read}, rather than the practical pulse interval, the scan-reading error t_{sr} is introduced, which is defined as the time from V_{INV} flipping to V_{INV} arriving at the column bus. According to the different positions of the V_{INV} signal, t_{sr} can be classified into three conditions as shown in Fig. 3.

Total Error Introduced by Synchronous Reading Mechanism: The total error introduced by the synchronous reading mechanism is defined as $t_{syn} + t_{sr}$, which can be divided into 12 types listing in Table 1.

The quantization error introduced by synchronous reading mechanism E_1 is expressed by:

$$E_1 = \frac{I_{in} - I_{out}}{I_{out}} \tag{2}$$

where I_{in} is the input photocurrent and I_{out} is the output photocurrent (only the errors introduced by the synchronous reading mechanism are taken into account). The following analysis illustrates the relationship between E_1 and other parameters by means of mathematical analysis and model simulation.

TABLE 1. **Total error introduced by synchronous reading mechanism.**

	t_{sr}(a)	t_{sr}(b)	t_{sr}(c)
t_{syn}(a)	$T_{LA}/4$	$(2N-3)T_{LA}/4$	$5T_{LA}/4$ to $(2N-7)T_{LA}/4$
t_{syn}(b)	$T_{LA}/4$	$(2N+1)T_{LA}/4$	$9T_{LA}/4$ to $(2N-3)T_{LA}/4$
t_{syn}(c)	$T_{LA}/4$ to $3T_{LA}/4$	$(2N-3)T_{LA}/4$ to $(2N-1)T_{LA}/4$	$5T_{LA}/4$ to $(2N-5)T_{LA}/4$
t_{syn}(d)	$3T_{LA}/4$ to $5T_{LA}/4$	$(2N-1)T_{LA}/4$ to $(2N+1)T_{LA}/4$	$7T_{LA}/4$ to $(2N-3)T_{LA}/4$

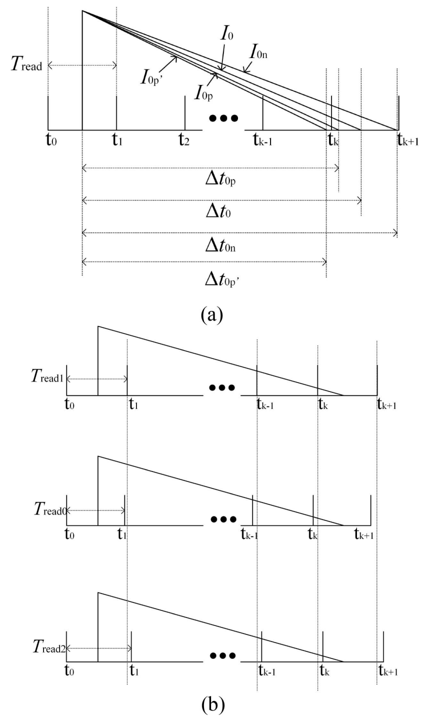

FIGURE 4. **Principle of estimating E_1 with reading period and relevant parameter. (a) Δt modified by the changing photocurrent. (b) It shows the change of T_{read} makes E_1 varies.**

Combined with (1), (2) can be rewritten as:

$$E_1 = 1 - \frac{C_{ph}(V_{rst} - V_{ref})/T\mathrm{all}}{C_{ph}(V_{rst} - V_{ref})/\Delta t} = 1 - \frac{\Delta t}{T_{all}} \tag{3}$$

where T_{all} is the reading interval between adjacent pulses (which is an integer multiple of the reading period T_{read}). When $(k-1/2)T_{read} < \Delta t < (k+1/2)T_{read}$, $T_{all} = kT_{read}$. Assuming that the initial photocurrent is I_0 in Fig. 4(a), we can get $T_{all} = \Delta t = kT_{read}$, and $E_1 = 0$ from (3). As I_0 decreases to I_{0n}, Δt_0 increases to Δt_{0n} and $kT_{read} = \Delta t_0 < \Delta t_{0n} < (k+1/2)T_{read}$, T_{all} remains constant. Equation (3) yields that E_1 decreases and its minimum value is $-1/(2k)$. Then I_0 increases to I_{0p}, Δt_0 decreases to Δt_{0p} and $(k-1/2)T_{read} < \Delta t_{0p} < \Delta t_0 = kT_{read}$, T_{all} remains constant. Similarly, from (3), we can yield that E_1 increases and its maximum value is $1/(2k)$. Therefore, when Δt is modified by the change of light intensity and $(k-1/2)T_{read} < \Delta t < (k+1/2)T_{read}$, the variation range of E_1 is $[-1/(2k), 1/(2k)]$. However, when I_{0p} increases to $I_{0p'}$, Δt_{0p} decreases to $\Delta t_{0p'}$

and $(k-3/2)T_{\text{read}} < \Delta t_{0p'} < \Delta t_{0p} < (k-1/2)T_{\text{read}}$, T_{all} decreases to $(k-1)T_{\text{read}}$. Then E_1 is greatly reduced and its variation range is $[-1/(2k-2), 1/(2k+2)]$. Therefore, it can be concluded that the increase of I_{ph} would make E_1 to periodic fluctuate approximately. In addition, E_1 and its fluctuation range gradually increase in each cycle. Besides, the simulation results of I_{ph} and E_1 (illustrated in Fig. 5(a)) show that with the increase of I_{ph}, E_1 approximates periodic fluctuations and the fluctuation range gradually increases, which is in accordance with above analysis.

From $C_{\text{pd}}V_{\text{diff}} = I_{\text{ph}}\Delta t$, where $V_{\text{diff}} = V_{\text{rst}} - V_{\text{ref}}$, we note that the increase in V_{diff} is equivalent to the decrease in I_{ph}, so we can conclude that as V_{diff} increases, the fluctuation of E_1 gradually reduces, which is confirmed by the simulation result in Fig. 5(b).

Since $T_{\text{all}} = \text{n}T_{\text{read}}$, (3) can be rewritten as:

$$E_1 = 1 - \frac{\Delta t}{nT_{\text{read}}} \tag{4}$$

where n is the number of T_{read} included in the reading interval. The initial reading period is T_{read1} in Fig. 4(b), $\Delta t = kT_{\text{read1}} = T_{\text{all}}$, and $E_1 = 0$. T_{read1} reduces to T_{read0} and $\Delta t/(k+1/2) < T_{\text{read0}} < T_{\text{read1}} = \Delta t/k$, since n and Δt remains unaltered, E_1 decreases and its minimum value is $-1/(2k)$. T_{read1} increases to T_{read2}, $\Delta t/k{=}T_{\text{read1}} < T_{\text{read2}} < \Delta t/(k-1/2)$. Since n and Δt remains unaltered, E_1 increases and its maximum value is $1/(2k)$. When n starts to decrease caused by the change of T_{read}, E_1 reduces severely, then the above cycle will be repeated until n changes again. When T_{read} increases from $\Delta t/(k-1/2)$ to $\Delta t/(k-3/2)$, the fluctuation range of E_1 is $[-1/(2k-2), 1/(2k-2)]$. Therefore, with the increase of T_{read}, E_1 fluctuates periodically, and its fluctuation range gradually extends, which is confirmed by the simulation results, shown in Fig. 5(c).

B. NON-LINEAR RESPONSE

Under the ideal linear response condition, the capacitance of the photodiode C_{pd} is fixed. However, C_{pd} changes by the photodiode node voltage V_{d} in photoelectric integral response and it can be given by:

$$C_{\text{pd}} = \frac{C_{\text{pd0}}}{(1+V_{\text{d}}/\phi_0)^m} \tag{5}$$

where C_{pd0} is the static capacitance of the photodiode, m is the slope coefficient, and ϕ_0 is the barrier voltage. The pulse interval time under linear response conditions T_{linear} and the pulse interval time under non-linear response conditions $T_{\text{nonlinear}}$ can be obtained:

$$T_{\text{linear}} = \frac{C_{\text{pd0}}(V_{\text{rst}} - V_{\text{ref}})}{(1+V_{\text{rst}}/\phi_0)^m I_{\text{ph}}} \tag{6}$$

$$\begin{aligned} T_{\text{nonlinear}} &= \frac{1}{I_{\text{ph}}}\int_{V_{\text{ref}}}^{V_{\text{rst}}} C_{\text{pd}}(V_{\text{d}})dV_{\text{d}} \\ &= \frac{C_{\text{pd0}}\phi_0}{I_{\text{ph}}(1-m)}\left[\left(1+\frac{V_{\text{rst}}}{\phi_0}\right)^{1-m} - \left(1+\frac{V_{\text{ref}}}{\phi_0}\right)^{1-m}\right]. \end{aligned} \tag{7}$$

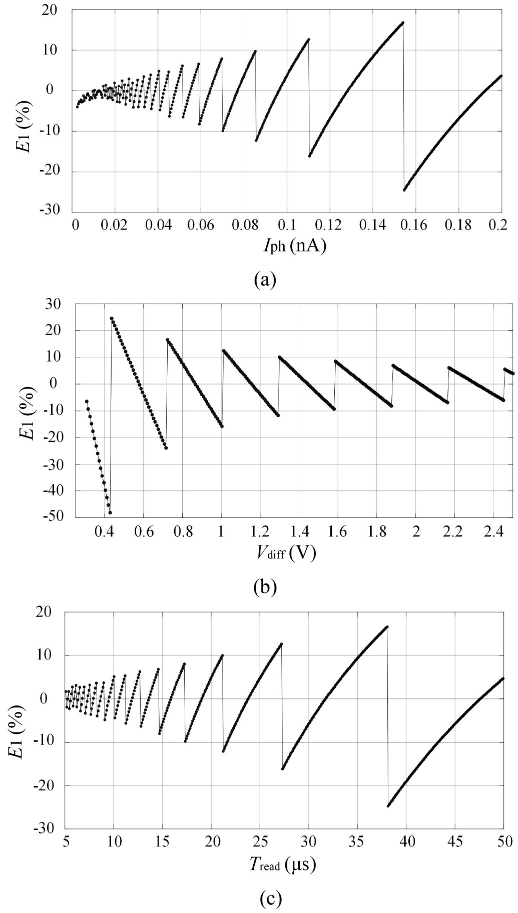

FIGURE 5. E_1 versus I_{ph}, V_{diff} and T_{read}. (a) E_1 versus I_{ph} ($V_{\text{diff}} = 2.2$V, $T_{\text{read}} = 25\mu$s). (b) E_1 versus V_{diff} ($T_{\text{read}} = 25\mu$s, $I_{\text{ph}} = 50$pA). (c) E_1 versus T_{read} ($V_{\text{diff}} = 1.1$V, $I_{\text{ph}} = 50$pA).

TABLE 2. Parameters defined in error model.

Parameters	Value
C_{pd0}	7fF
I_{ph}	250pA
V_{rst}	2.2-3.3V
V_{ref}	1.0-2.1V
ϕ_0	0.6-0.7V
m	0.25-0.5

Fig. 6 shows the deviation between the nonlinear curve and the linear curve, simulating with the integrated nonlinear error model, gradually increases with V_{d} decreases. The relevant parameters and values are listed in Table 2.

The quantization error E_2 introduced by the nonlinear response is defined as:

$$E_2 = \frac{T_{\text{nonlinear}} - T_{\text{linear}}}{T_{\text{linear}}} = \frac{\frac{\phi_0 Q}{1-m} - \left(1+\frac{V_{\text{d}}}{\phi_0}\right)^{-m} V_{\text{diff}}}{V_{\text{diff}}\left(1+\frac{V_{\text{rst}}}{\phi_0}\right)^{-m}} \tag{8}$$

where $Q = (1+\frac{V_{\text{rst}}}{\phi_0})^{1-m} - (1+\frac{V_{\text{ref}}}{\phi_0})^{1-m}$.

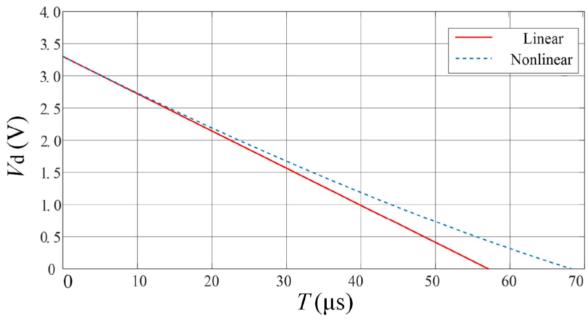

FIGURE 6. Simulation results of linear comparing with non-linear response.

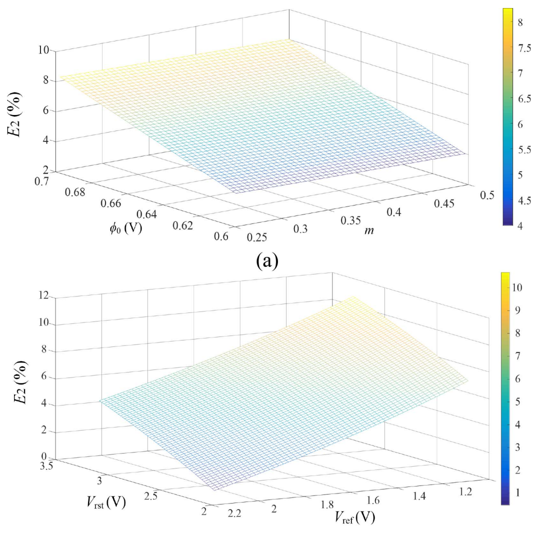

FIGURE 7. E_2 **versus** m **and** ϕ_0**. (a) Relation between** E_2**,** m **and** ϕ_0**. (b)** E_2 **with** $m = 0.27$**,** $\phi_0 = 0.7$**V.**

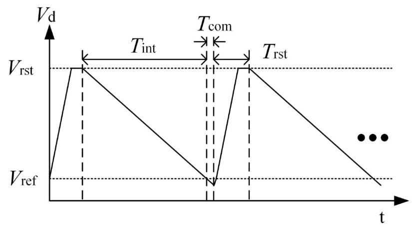

FIGURE 8. Timing diagram of integration process in practice.

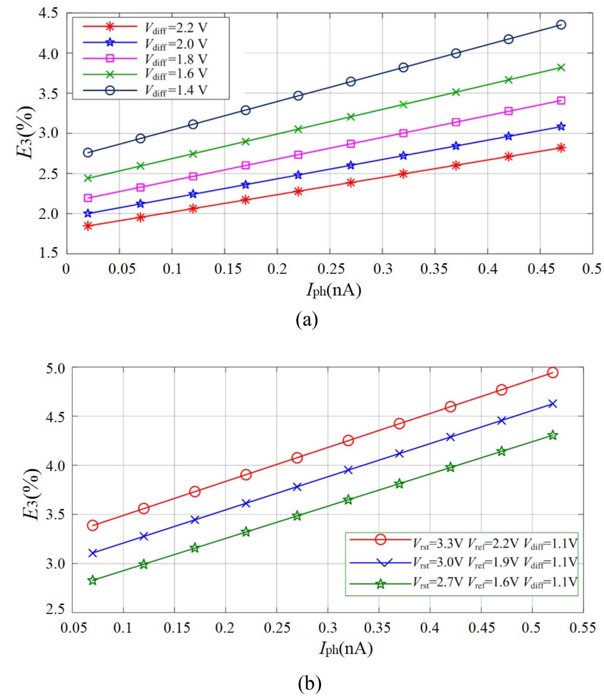

FIGURE 9. E_3 **versus** I_{ph}**,** V_{rst} **and** V_{ref}**. (a)** $V_{rst} = 3.3$**V. (b)** $V_{diff} = 1.1$**V.**

From (8) we can note that E_2 is independent of I_{ph} and C_{pd}, but dependent on V_{rst}, V_{ref}, m and ϕ_0. m and ϕ_0 are determined by the process. Fig. 7(a) illustrates that E_2 decreases with m and ϕ_0 decrease. The relationship between E_2 and voltages is shown in Fig. 7(b): E_2 decreases with V_{ref} and V_{rst} increase when V_{diff} is fixed, and E_2 increases with V_{diff} increases. In the error modeling analysis, we set $m = 0.27$, $\phi_0 = 0.7$ V according to the process.

C. COMPARATOR DELAY ERROR

The ideal comparator is activated when V_d drops to the comparator reference voltage V_{ref}. However, in practice, the limited DC gain of the comparator and the output slew rate make the comparator activated when V_d decrease slightly smaller than V_{ref}, where introduce the comparator delay T_{com}. Fig. 8 illustrates the concept. The operation cycle includes three parts: integration time T_{int}, comparator delay T_{com}, and pixel reset time T_{rst}. If T_{com} and T_{rst} are ignored when quantizing the light intensity, quantization error will be introduced.

Taking the static and dynamic characteristics of the comparator into considered, T_{com} can be express by the comparator reaction time T_{rea} and the transmission time T_{tra}. T_{rea} is given by:

$$T_{rea} = \frac{1}{I_{ph}} \int_{V_{ref}-V_{min}}^{V_{ref}} C_{pd0} \left(1 + \frac{V_d}{\phi_0}\right)^{-m} dV_d \tag{9}$$

where V_{min} is the minimum input voltage that the comparator can detect. V_{min} equals to $(V_h - V_l)/A$, where A is the DC gain of the comparator, V_h and V_l are high level and low level of the comparator output, respectively. Equation (9) can be rewritten as:

$$T_{rea} = \frac{C_{pd0}\phi_0}{I_{ph}(1-m)} \times \left[\left(1 + \frac{V_{ref}}{\phi_0}\right)^{1-m} - \left(1 + \frac{V_{ref}A - V_{rst}}{A\phi_0}\right)^{-m}\right]. \tag{10}$$

The comparator transmission time, $T_{tra} = \tau c \ln 2$, where τc is time constant of the step signal which is given to the comparator. Then we can get

$$\begin{aligned} T_{\mathrm{com}} &= T_{\mathrm{rea}} + T_{\mathrm{tra}} \\ &= \frac{C_{\mathrm{pd0}}\phi_0}{I_{\mathrm{ph}}(1-m)} \\ &\times \left[\left(1+\frac{V_{\mathrm{ref}}}{\phi_0}\right)^{1-m} - \left(1+\frac{V_{\mathrm{ref}}A - V_{\mathrm{rst}}}{A\phi_0}\right)^{-m}\right] \\ &= \tau c \ln 2. \end{aligned} \tag{11}$$

The reset time T_{rst} also introduces quantization errors theoretically. Since reset and reading are performed simultaneously, the effect of T_{rst} will be covered by the error of the synchronous reading.

The quantization error E_3 introduced by the comparator delay T_{com} is defined as:

$$E_3 = \frac{T_{\mathrm{com}}}{T_{\mathrm{com}} + T_{\mathrm{int}}}. \tag{12}$$

Fig. 9 shows simulation results using an error model to estimate the quantization error E_3 introduced by the comparator delay. It can be found from the plot that E_3 increases with the increase of I_{ph}. For the same I_{ph}, E_3 decreases with the increase of V_{diff}. For the same V_{diff}, E_3 decreases as V_{rst} and V_{ref} decrease. Therefore, under the condition of larger V_{diff}, V_{rst} and V_{ref} should be as small as possible to suppress the quantization error caused by the comparator delay.

D. ENTIRE QUANTIZATION ERROR

The sensor's entire quantization error E_{all} is defined as:

$$E_{\mathrm{all}} = \frac{I_{\mathrm{inp}} - I_{\mathrm{outp}}}{I_{\mathrm{inp}}} \tag{13}$$

where I_{inp} is the input photocurrent, and I_{outp} is the output photocurrent after quantization by the sensor. Fig. 10(a) shows that with the increase of I_{ph}, the fluctuation range of E_{all} extends rapidly. Fig. 10(b) shows the relationship between E_{all}, V_{ref} and V_{rst}. If V_{diff} keeps fixed, E_{all} gradually decreases as V_{ref} and V_{rst} increase. Fig. 10(c) shows that as T_{read} increases, the fluctuation range of E_{all} broadens rapidly.

IV. EXPERIMENTAL RESULTS

To validate the above analysis and the error model, we tested response and quantization error by means of the synchronous PWM image sensor [5], [18], which has the reset voltage adjusting from 2.4V to 3.3V continuously. The reference voltage is ten-level adjustable from 1.05V to 2.32V, and the testing intensity is 50lux to 800lux. Table 3 gives the relevant parameters of the chip.

In (13), the input and output are photocurrents, while light intensity and photocurrent after quantization are considered as the input and output of the sensor during testing, respectively. The input light intensity needs to be converted into the input photocurrent with the equation:

$$I_{\mathrm{ph}} = \eta K \tag{14}$$

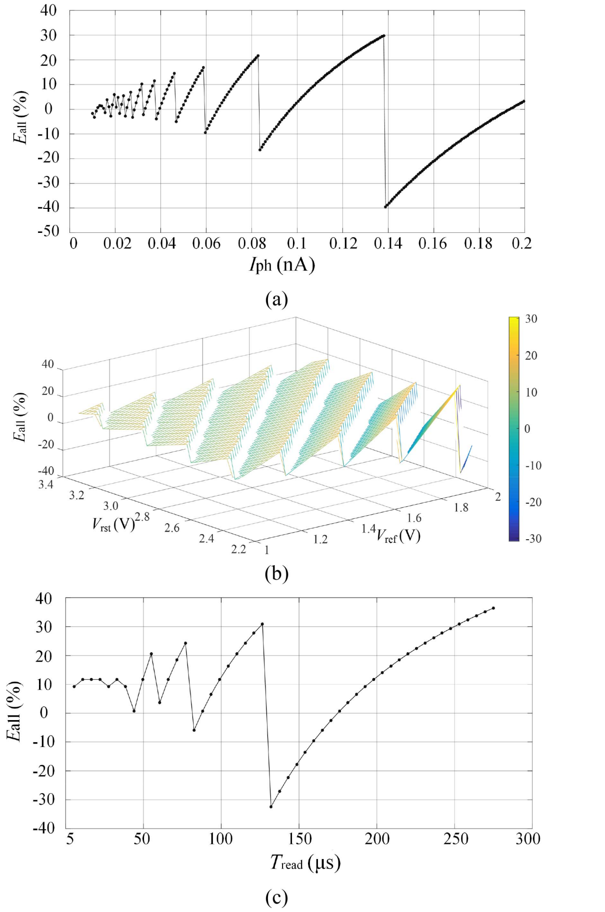

FIGURE 10. E_{all} versus I_{ph}, V_{rst}, V_{ref} and T_{read}. (a) E_{all} versus I_{ph} ($V_{\mathrm{rst}} = 3.3$V, $V_{\mathrm{ref}} = 2.2$V, $T_{\mathrm{read}} = 25\mu$s). (b) E_{all} versus V_{rst} and V_{ref} ($T_{\mathrm{read}} = 25\mu$s, $I_{\mathrm{ph}} = 50$ pA). (c) E_{all} versus T_{read} ($I_{\mathrm{ph}} = 50$pA, $V_{\mathrm{rst}} = 3.3$V, $V_{\mathrm{ref}} = 2.2$V).

TABLE 3. Summary of parameters in testing sensor.

Parameters	Value
Supply Voltage	3.3V(Analog),1.5V(Digital)
Pixel Array	400(H)×250(V)
Pixel size	20μm×20μm
Fill Factor	13.75%
Light Intensity	50lux-800lux
Frame Rate	800fps-40Kfps
Time Resolution	25μs
Readout Interface	LVDS(8 Lane)/500MHz
Data Rate	4Gbps@40Kfps
V_{rst}	2.4V-3.3V
V_{ref}	1.05V-2.32V
T_{read}	25μs-1250μs

where η is the conversion factor and K is the illuminance. η is defined by photocurrent and integrated falling time T_{read}, which is the corresponding to the maximum illuminance that sensor can detect with fixed T_{read}, T_{rst} and T_{ref} .

Fig. 11 shows the comparison between simulation and testing results, from where we can note the testing results are

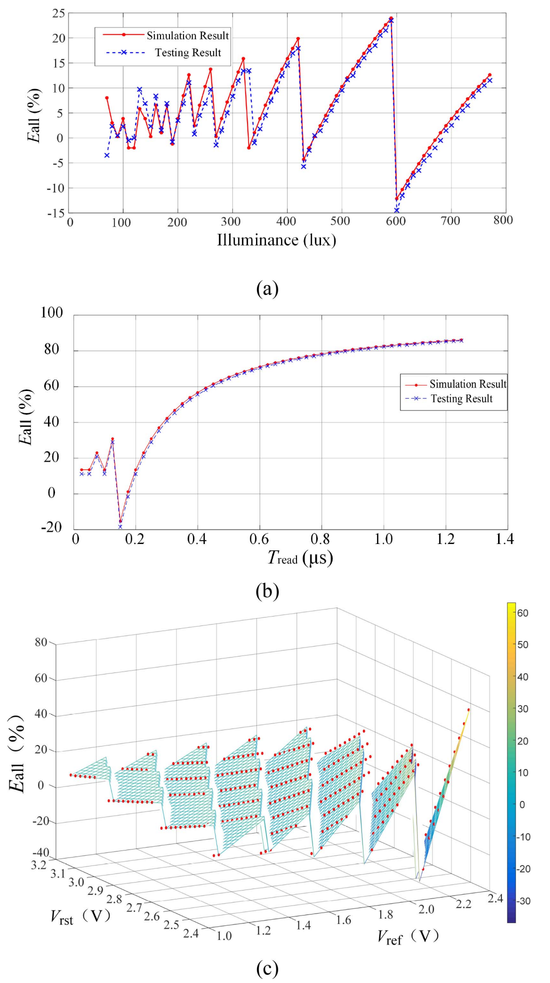

FIGURE 11. Total quantization error comparing simulation and testing results. The red dots present the testing result. (a) E_{all} versus illuminance ($V_{rst} = 3.3V$, $V_{ref} = 1.3V$, $T_{read} = 25\mu s$). (b) E_{all} versus T_{read} ($V_{rst} = 3.3V$, $V_{ref} = 1.3V$, $K = 300lux$). (c) E_{all} versus V_{rst} and V_{ref} ($T_{read} = 25\ \mu s$, $K = 300lux$).

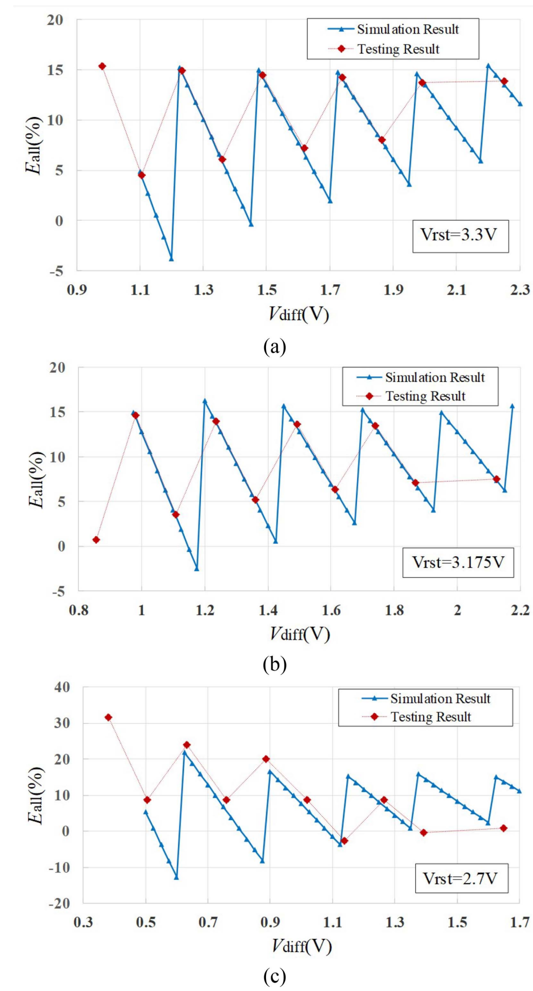

FIGURE 12. With $T_{read} = 25\ \mu s$, $K = 300lux$, total quantization error comparing simulation and testing results. (a) $V_{rst} = 3.3V$ (b) $V_{rst} = 3.175V$. (c) $V_{rst} = 2.7V$. We can observe that the bigger V_{rst} has the better simulation performance comparing with the testing result.

basically consistent with the simulation ones. Fig. 11(a) and Fig. 11(b) show that with the increase of T_{read} or illuminance, the fluctuation range of E_{all} extends gradually.

Using the data collected in Fig. 11(c), we compare E_{all} with different V_{diff} and a constant T_{read} and illuminance. As shown in Fig. 12, the simulation result curve of 3.3V and 3.175V are much closer to the testing result curve than the result of 2.7V because the bigger V_{rst} can ensure the bigger Δt with the fixed I_{ph}, which means a more precisely interval time to make the error model functioning well. The V_{ref} of the sensor which has ten-level adjustable makes the testing result taking ten values on the x-axis. Even that, the trend of testing result proves the simulation model effectively. Since V_{diff} is the difference between V_{rst} and V_{ref}, the influence of V_{rst} and V_{ref} on the error is relatively complicated than other parameters. We can find from the figures and the following conclusions can be drawn: E_{all} decreases with V_{rst} and V_{ref} increases when V_{diff} is fixed. The effect of comparator delay and synchronous reading mechanism on E_{all} is greater than the nonlinear response, resulting in the fluctuation of E_{all} gradually decreases as V_{diff} increases. Hence, V_{ref} should be set as large as possible in the condition of satisfying larger V_{diff} to suppress the fluctuation of E_{all}. Therefore, for the suppressing of the fluctuation of E_{all}, a bigger V_{rst}, a smaller V_{ref} and T_{read} should be chosen to achieve the little and stable quantization error.

V. CONCLUSION

A new estimation approach of the light intensity quantization error in PWM image sensor is presented. The quantization error takes non-linear response, comparator delay and synchronous reading mechanism into account. The proposed model, showing the relation between the total quantization error and the pixel parameters including I_{ph}, V_{rst}, V_{ref}, V_{diff} and T_{read}, is operated on a PWM image sensor, and the testing results prove the model effectively. In the condition of $V_{rst} = 3.3V$, $V_{ref} = 2.2V$, $T_{read} = 25\mu s$, when the illuminance ranges from 100lux to 600lux, the fluctuation range of the total quantization error broadens from (0.1%-4%) to

(−5%-24%) . In addition, with 300lux and $T_{\text{read}} = 25\mu\text{s}$, the appropriate V_{rst} and V_{ref} can be chosen to obtain the smallest fluctuation range (11%-15%) with the model. The model proposed in this article can be employed in pulse width image sensor designing for suppressing the fluctuation of the quantization error to optimize the image sensor system design.

REFERENCES

[1] S. Chen, A. Bermak, and F. Boussaid, "A compact reconfigurable counter memory for spiking pixels," *IEEE Electron Device Lett.*, vol. 27, no. 4, pp. 255–257, Apr. 2006.

[2] C. Shoushun, F. Boussaid, and A. Bermak, "Robust intermediate read-out for deep submicron technology CMOS image sensors," *IEEE J. Sensors*, vol. 8, no. 3, pp. 286–294, Mar. 2008.

[3] E. Culurciello, R. Etienne-Cummings, and K. Boahen, "Arbitrated address-event representation digital image sensor," *Electron. Lett.*, vol. 37, no. 24, pp. 1443–1445, Nov. 2001.

[4] E. Culurciello, R. Etienne-Cummings, and K. A. Boahen, "A biomorphic digital image sensor," *IEEE J. Solid-State Circuits*, vol. 38, no. 2, pp. 281–294, Feb. 2003.

[5] G. Jing, W. Yanzhao, N. Kaiming, and G. Zhiyuan, "The analysis and suppressing of non-uniformity in a high-speed spike-based image sensor," *Sensors*, vol. 18, pp. 4232–4252, Dec. 2018.

[6] J. A. Leñero-Bardallo, T. Serrano-Gotarredona, and B. Linares-Barranco, "A five-decade dynamic-range ambient-light-independent calibrated signed-spatial-contrast AER retina with 0.1-ms latency and optional time-to-first-spike mode," *IEEE Trans. Circuits Syst. I, Reg. Papers*, vol. 57, no. 10, pp. 2632–2643, Oct. 2010.

[7] K. Cho, S. Lee, O. Kavehei, and K. Eshraghian, "High fill factor low-voltage CMOS image sensor based on time-to-threshold PWM VLSI architecture," *IEEE Trans. Very Large Scale Integr. (VLSI) Syst.*, vol. 22, no. 7, pp. 1548–1556, Jul. 2014.

[8] C. Posch, D. Matolin, and R. Wohlgenannt, "A QVGA 143 dB dynamic range frame-free PWM image sensor with lossless pixel-level video compression and time-domain CDS," *IEEE J. Solid-State Circuits*, vol. 46, no. 1, pp. 259–275, Jan. 2011.

[9] K. A. Boahen, "A burst-mode word-serial address-event link-II: Receiver design," *IEEE Trans. Circuits Syst. I, Reg. Papers*, vol. 51, no. 7, pp. 1281–1291, Jul. 2004.

[10] J. A. Leñero-Bardallo, R. Carmona-Galán, and Á. Rodríguez-Vázquez, "A wide linear dynamic range image sensor based on asynchronous self-reset and tagging of saturation events," *IEEE J. Solid-State Circuits*, vol. 52, no. 6, pp. 1605–1617, Jun. 2017.

[11] J. A. Leñero-Bardallo, F. Pérez-Peña, R. Carmona-Galán, and Á. Rodríguez-Vázquez, "Pipeline AER arbitration with event aging," in *Proc. IEEE Int. Conf. Symp. Circuits Syst.*, Baltimore, MD, USA, 2017, pp. 1–4.

[12] X. Peng, B. Zhao, R. Yan, H. Tang, and Z. Yi, "Bag of events: An efficient probability-based feature extraction method for AER image sensors," *IEEE Trans. Neural Netw. Learn. Syst.*, vol. 28, no. 4, pp. 791–803, Apr. 2017.

[13] X. Guo, X. Qi, and J. G. Harris, "A time-to-first-spike CMOS image sensor," *IEEE J. Sensors*, vol. 7, no. 8, pp. 1165–1175, Aug. 2007.

[14] J. P. Crooks *et al.*, "A CMOS image sensor with in-pixel ADC, timestamp, and sparse readout," *IEEE J. Sensors*, vol. 9, no. 1, pp. 20–28, Jan. 2009.

[15] X. Jiangtao, M. Jin, G. Zhiyuan, N. Kaiming, and S. Xiaopei, "Analysis and modeling of quantization error in spike-frequency-based image sensor," *Microelectron. Rel.*, vol. 111, Aug. 2020, Art. no. 113705.

[16] A. Kitchen, A. Bermak, and A. Bouzerdoum, "A digital pixel sensor array with programmable dynamic range," *IEEE Trans. Electron Devices*, vol. 52, no. 12, pp. 2591–2601, Dec. 2005.

[17] A. Bermak and Y.-F. Yung, "A DPS array with programmable resolution and reconfigurable conversion time," *IEEE Trans. Very Large Scale Intergr. (VLSI) Syst.*, vol. 14, no. 1, pp. 15–22, Jan. 2006.

[18] J. Xu, Z. Yang, Z. Gao, W. Zheng, and J. Ma, "A method of biomimetic visual perception and image reconstruction based on pulse sequence of events," *IEEE J. Sensors*, vol. 19, no. 3, pp. 1008–1018, Feb. 2019.

SILU CHENG received the B.E. and M.S. degrees from the School of Electronic Information Engineering, Tianjin University, China, in 2012 and 2015, respectively, where she is currently pursuing the Doctoral degree with the School of Microelectronics. Her research interests include dynamic image sensor and spiking neural network.

JIANGTAO XU (Member, IEEE) received the B.E., M.S., and Ph.D. degrees from the School of Electronic Information and Engineering, Tianjin University, China, in 2001, 2004, and 2007, respectively. From 2007 to 2010, he was a Lecturer and from 2010 to 2018, he was an Associate Professor with the School of Electronic Information Engineering, Tianjin University, where he is currently working as an Professor with the School of Microelectronics. His research interests include CMOS image sensor and digital image signal processing system.

ZHIYUAN GAO (Member, IEEE) received the B.E. and Ph.D. degrees from the School of Electronic Information Engineering, Tianjin University, Tianjin, China, in 2010 and 2015, respectively, where he is currently working as an Assistant Professor. His current research interests include CMOS image sensor design especially on pixel design, dynamic range enhancement, and bionic CISs.

KAIMING NIE (Member, IEEE) received the B.E., M.S., and Ph.D. degrees from the School of Electronic Information and Engineering, Tianjin University, Tianjin, China, in 2009, 2011, and 2014, respectively, where he was a Postdoctoral Fellow, from July 2014 to September 2017. Since September 2017, he has been an Associate Professor with the School of Microelectronics, Tianjin University. His research interests are in mixed analog/digital circuit design and CMOS image sensor design.

XIAOPEI SHI received the B.E. degree from the School of Microelectronics, Tianjin University, Tianjin, China, in 2018, where she is currently pursuing the master's degree. Her current research interests include image processing and high frame rate video reconstruction based on event camera.

JIN MIAO received the B.E. and M.S. degrees from the School of Microelectronics, Tianjin University, Tianjin, China, in 2017 and 2020, respectively. His research interests are in analog circuit design for CMOS image sensor.